Magnetic Compton profiles of Fe and Ni corrected by dynamical electron correlations

D. Benea,[1] J. Minár,[2] L. Chioncel,[3,4] S. Mankovsky,[2] and H. Ebert[2]

[1]*Faculty of Physics, Babes-Bolyai University, Kogalniceanu Str. 1, Ro-400084 Cluj-Napoca, Romania*

[2]*Chemistry Department, University Munich, Butenandstrasse 5-13, D-81377 München, Germany*

[3]*Augsburg Center for Innovative Technologies, University of Augsburg, D-86135 Augsburg, Germany*

[4]*Theoretical Physics III, Center for Electronic Correlations and Magnetism, Institute of Physics, University of Augsburg, D-86135 Augsburg, Germany*

(Received 21 October 2011; revised manuscript received 1 February 2012; published 13 February 2012)

Magnetic Compton profiles (MCPs) of Ni and Fe along the [111] direction have been calculated using a combined density functional and many-body theory approach. At the level of the local spin density approximation, the theoretical MCPs do not describe correctly the experimental results around the zero momentum transfer. In this work, we demonstrate that inclusion of electronic correlations as captured by dynamical mean-field theory (DMFT) improves significantly the agreement between the theoretical and the experimental MCPs. In particular, an energy decomposition of Ni MCPs gives an indication of spin polarization and the intrinsic nature of the Ni 6 eV satellite, a genuine many-body feature.

DOI: 10.1103/PhysRevB.85.085109 PACS number(s): 71.15.Mb, 71.20.Be, 75.30.−m

I. INTRODUCTION

Magnetic Compton scattering is a well-established technique for probing the spin-dependent momentum densities of magnetic solids.[1,2] Compared with other experimental techniques, Compton scattering offers several advantages. Compton scattering is an inelastic process, in which an energetic photon collides with a single electron and transfers energy to it. Since the scattering is from a single electron and (to a good approximation) occurs at a single point in space, the process must be incoherent and is supplying an average over real space. Therefore, Compton scattering is related directly to the electronic ground state, whereas other spectroscopic methods (e.g., photoemission spectroscopy) involve excited states.

In addition, Compton scattering allows for a rather fundamental test of the theories used to describe the spin-dependent momentum density, since these theoretical methods are tailored to give predictions for the ground-state properties. Several theoretical methods have been used in the past to describe the electron momentum density and to analyze the experimental magnetic Compton profiles (MCPs).[3–9] Most of the corresponding calculations were done within the local spin density approximation (LSDA) for the exchange-correlation potential. In general, the theoretical profiles obtained using the LSDA show an overall agreement with the experimental measurements, except within the region $p_z < 1$ a.u. Recently, several theoretical methods beyond the LSDA have been applied in order to describe the features of the MCP that cannot be explained using the LSDA-based approach and to improve the agreement with experiment.[6–8,10,11] Dixon *et al.*[7] and Baruah *et al.*[6] compared the generalized gradient approximation (GGA) and LSDA methods, using the linear muffin tin orbital (LMTO) and full potential linearized augmented plane wave (FLAPW) methods, respectively, and a dense **k**-point mesh. They showed that GGA calculations improve the MCP of Ni in the low momentum region where the negative polarization of *s* and *p* electrons becomes significant.

At the same time, it was pointed out that the discrepancy between the experimental and theoretical MCP could be attributed to missing electron-electron correlations in band models.[12] Along these lines, recently, the LSDA+*U* method was applied by Tokii *et al.*[8] to calculate the MCPs of Fe, showing improvement for the [100] and [110] directions, but it still underestimates near the origin the MCP for the [111] direction. Also, one should mention the calculations of the Ni MCP done by Kubo[10] implemented within the *GW* scheme based on the FLAPW method. His calculations are in overall agreement with experiment, but notable discrepancies are still found for the Ni [110] and [111] MCP spectra.

The electronic structure of fcc Ni has been a subject of intensive studies as a prototype of itinerant electron ferromagnets, since they indicate a failure of the one-electron theory.[13–16] The LSDA calculations for fcc Ni cannot reproduce some features of the electronic structure of Ni observed experimentally. The valence-band photoemission spectra of Ni (Refs. 17 and 18) show a 3*d*-band width that is about 30% narrower than obtained from the LSDA calculations.[15] Second, the spectra show a dispersionless feature at about 6 eV binding energy (the so-called 6 eV satellite),[19,20] which again cannot be reproduced by the LSDA calculations. Third, the magnetic exchange splitting is overestimated by the LSDA calculations[15] compared with the experimental data.[21] On the other hand, an improved description of the correlation effects for the 3*d* electrons via the LSDA+DMFT[22–25] gives the width of the occupied 3*d* bands of Ni properly and reproduces the exchange splitting and the 6 eV satellite structure in the valence band.

In view of these LSDA+DMFT improvements[22,23,26] upon the magnetic properties of Fe and Ni, the comparison of experimental MCP with the LSDA+DMFT theory provides some new information besides offering a test for the impact of electronic correlations. In particular, we demonstrate here that the LSDA+DMFT calculations improve also the agreement between theory and experiment for Fe and Ni MCPs. In the following, we briefly discuss the theoretical approach and present the calculated MCPs of Fe and Ni together with the experimental data. Finally, the LSDA and LSDA+DMFT calculated MCPs of Ni have been decomposed and the

contribution of different energy windows in the valence band have been compared in order to extract the features of electron correlations and to show their energy dependency. Such a decomposition provides evidence of the connection between the MCP contribution in the lower part of the valence band and the existence of the 6 eV satellite, both features being captured only within LSDA+DMFT.

II. THEORETICAL FRAMEWORK

The calculations were done using the spin-polarized relativistic Korringa-Kohn-Rostoker (SPR-KKR) method in the atomic spheres approximation (ASA).[27] The computational scheme is based on the KKR Green function formalism, which makes use of multiple scattering theory, and was recently extended to compute MCPs.[28–30] The spin-projected momentum density $n_{m_s}(\vec{p})$ [where $m_s = \uparrow (\downarrow)$] is computed using the LSDA(+DMFT) Green's functions in momentum space as

$$n_{m_s}(\vec{p}) = -\frac{1}{\pi}\int_{-\infty}^{E_F} \mathrm{Im}G_{m_s}^{\mathrm{LSDA(+DMFT)}}(\vec{p},\vec{p},E)dE.$$

In order to analyze the momentum density and the corresponding MCPs in different energy ranges, we use a decomposition of the above formula in the form

$$n_{m_s,\Delta E}(\vec{p}) = -\frac{1}{\pi}\int_{E_1}^{E_2} \mathrm{Im}G_{m_s}^{\mathrm{LSDA(+DMFT)}}(\vec{p},\vec{p},E)dE,$$

where $\Delta E = E_2 - E_1$ represents the width of the energy window. The MCP seen in each energy window ΔE is obtained by performing a double integral in the momentum plane perpendicular to the scattering momentum $\vec{p}_z$,

$$J_{\mathrm{mag}}^{\mathrm{LSDA(+DMFT)}}(p_z) = \iint [n_\uparrow(\vec{p}) - n_\downarrow(\vec{p})]dp_x dp_y.$$

Here the electron momentum density for a given spin orientation is given by $n_{\uparrow(\downarrow)}(\vec{p})$. The area under the MCP is equal to the spin moment per Wigner-Seitz cell: $\int_{-\infty}^{+\infty} J_{\mathrm{mag}}^{\mathrm{LSDA(+DMFT)}}(p_z)dp_z = \mu_{\mathrm{spin}}^{\mathrm{LSDA(+DMFT)}}$. In the actual calculations, the experimental lattice parameters of Fe and Ni have been used ($a_{\mathrm{Fe/Ni}} = 0.287/0.352$ nm). The exchange-correlation potentials parametrized by Vosko, Wilk, and Nusair[31] were used for the LSDA calculations. For integration over the Brillouin zone, the special points method has been used.[32] In addition to the LSDA calculations, a charge and self-energy self-consistent scheme for correlated systems based on the KKR approach with the many-body effects described by the means of DMFT has been applied.[23] As a DMFT solver, the relativistic version of the so-called spin-polarized T-matrix fluctuation exchange approximation[33,34] was used. The realistic multiorbital interaction has been parametrized by the average screened Coulomb interaction U and the Hund exchange interaction J. The values of U and J are sometimes used as fitting parameters, although recent developments enable us to compute the dynamic electron-electron interaction matrix elements exactly.[35] As it was shown, the static limit of the screened-energy-dependent Coulomb interaction leads to a U parameter in the energy range of 2–3 eV for all $3d$ transition metals. As the J parameter is not affected by screening, it can be calculated directly within the LSDA and is approximately the same for all $3d$ elements ≈ 0.9 eV. In our calculations, we used the values $U = 2.0$ (2.3) eV for Fe (Ni) and the same value of the Hund exchange interaction $J = 0.9$ eV for both Fe and Ni. These parameters were chosen based on previous calculations that combine at best the results of structural and spectroscopical analysis performed on Fe and Ni.[22,33,36] In addition, we have performed MCP calculations of Fe and Ni for values in the range of 2–3 eV and checked that for larger values of U, the correlation effects are overestimated, in agreement with the structural analysis.[36]

III. RESULTS AND DISCUSSIONS

The MCPs of Ni [111] calculated on the basis of the LSDA and LSDA+DMFT, respectively, are shown in Fig. 1, together with the experimental data. The Gaussian broadening applied to the calculated MCPs corresponds to the experimental resolution. The experimental MCPs stemming from Dixon *et al.*[7] have been normalized to the experimentally determined spin moment ($0.56\mu_B$). After broadening, the calculated KKR MCP spectra have been normalized to the calculated spin moment ($0.6\mu_B$ by LSDA and LSDA+DMFT).

As can be seen, in the high-momentum region ($p_z \geqslant 2$ a.u.) the correlation effects have a small influence on the magnetic spin density. In the momentum region $0 \leqslant p_z \leqslant 2$ a.u., taking into account the electron correlations by the LSDA+DMFT approach improves the agreement with the experimental spectra considerably. Our LSDA+DMFT calculations can reproduce the dip in the [111] profile at ~ 0.8 a.u., which was clearly underestimated by the LSDA calculations.

The LSDA and LSDA+DMFT calculated MCPs of Fe [111] are shown in Fig. 2 together with the experimental spectra of McCarthy *et al.*[37] The experimental MCP has been normalized to a spin momentum of $2.07\mu_B$. The calculated spectra have been convoluted with a Gaussian of 0.42 a.u., corresponding to the experimental resolution. After convolution, the calculated MCPs have been scaled at a spin momentum of $2.3\mu_B$ (the LSDA calculated MCP) and

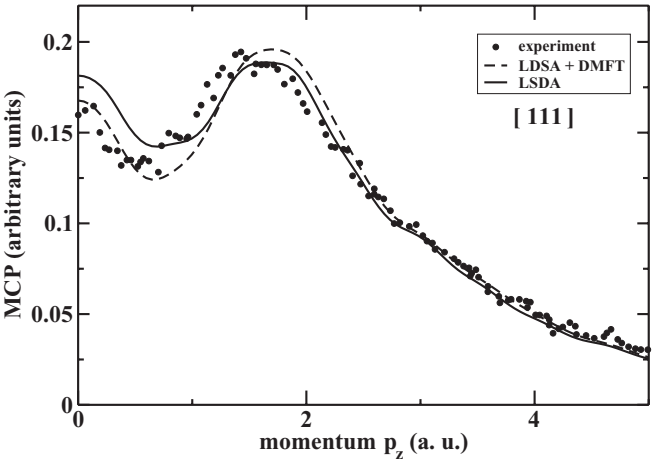

FIG. 1. MCPs of Ni [111] calculated via the KKR method within the LSDA and LSDA+DMFT approach. The theoretical curves have been convoluted with a Gaussian of 0.43 a.u. FWHM, corresponding to the experimental resolution. The experimental data stem from Dixon *et al.*[7]

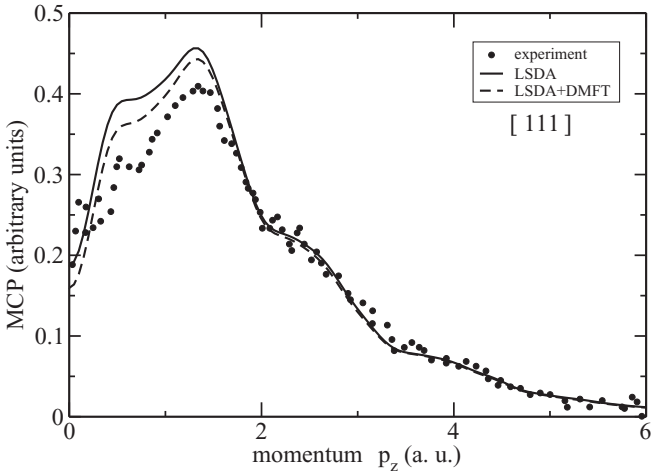

FIG. 2. MCPs of Fe [111] calculated via the KKR method within the LSDA and LSDA+DMFT approach. The theoretical curves have been convoluted with a Gaussian of 0.42 a.u. FWHM, corresponding to the experimental resolution. The experimental data stem from McCarthy *et al*.[37]

$2.19\mu_B$ (the LSDA+DMFT calculated MCP), respectively. Although both calculated MCPs show agreement with the experiment in the high-momentum region, the shoulder at $\sim$ 0.5 a.u. is diminished in the LSDA+DMFT calculated MCP, improving the agreement with the experimental spectra also in the low-momentum region.

The theoretical MCP of Ni [111] has been decomposed into contributions from different energy windows. To illustrate the decomposition into energy windows, the LSDA calculated MCPs stemming from the energy bands below the Fermi level in the range [−0.4 Ry, E_F] and [−1.0 Ry, −0.4 Ry] are shown in Fig. 3. As can be seen, the main contribution of the LSDA calculated MCP stems from the energy bands situated between −0.4 Ry and the Fermi level. The bands at energy lower than −0.4 Ry have just a small positive contribution to the MCP within the momentum range $p_z \leqslant 1$ a.u. The corresponding decomposition has been performed

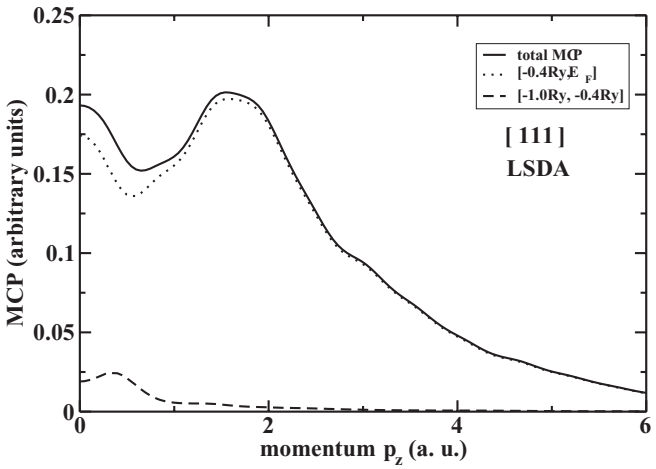

FIG. 3. The theoretical MCPs of Ni [111] obtained from LSDA calculations. The MCPs have been decomposed into contributions of two energy windows: [−1.0 Ry, −0.4 Ry] and [−0.4 Ry, E_F].

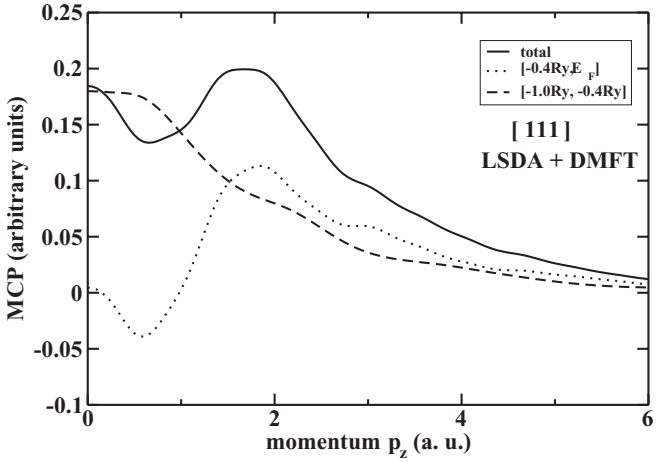

FIG. 4. The theoretical MCP of Ni [111] obtained from KKR LSDA+DMFT calculations. The MCPs have been decomposed into contributions of two energy windows: [−1.0 Ry, −0.4 Ry] and [−0.4 Ry, E_F].

as well for the LSDA+DMFT calculated MCP, and the results are shown in Fig. 4. The contribution of the energy bands situated between −0.4 Ry and the Fermi level has an important negative polarization for $p_z \leqslant 1$ a.u. According to the *s*-, *p*-, and *d*-electron decomposition (not shown here), the negative contribution stems from *s* and *p* electrons. The overall negative polarization of *s* and *p* electrons is increased in the LSDA+DMFT MCP compared with the LSDA approach. The importance of negative polarization was discussed also in the context of the previous GGA calculations,[6,7] where this feature is connected with the fact that the GGA favors inhomogeneity in the electron density. Including dynamic correlations, the spectral weight transfer of the *d* manifolds takes place, creating the 6 eV satellite and enhancing at the same time the negative *s* and *p* contribution.

An essential feature is the important positive contribution of the electronic states in the energy window [−1.0 Ry, −0.4 Ry] to the MCP, which is similar for different scattering directions. The MCP carries information about all spin-polarized electrons in the system and about their localization. A broad contribution in the MCP is an indication for dominating localized spin states.[1] As the LSDA+DMFT MCPs are broader than the LSDA ones, we have a clear indication that the spin magnetic densities have the tendency to localize in the presence of the electronic correlations. Previous LDA+DMFT implementations demonstrate in fact a reduced spatial extension of the computed spin densities.[26] As this MCP broadening is seen in the energy range [−1.0 Ry, −0.4 Ry] where the well-known feature of the correlated electronic bands of Ni, namely the 6 eV satellite (0.44 Ry), is situated, a direct connection between these two correlation features is presumable. As was shown by earlier calculations[22] and confirmed by photoemission experiments,[38] the 6 eV satellite is spin-polarized and accordingly has to be connected with the MCP. The general interpretation of the 6 eV satellite relates this feature to an excited state involving two 3*d* holes bound on the same Ni site, therefore it is not accessible to any LSDA calculations. In contrast, the LSDA+DMFT approach is able to capture such processes via the explicit existence within the

interacting Hamiltonian of the four-index form of the Coulomb matrix. Although the correlation-induced satellite is absent in Fe, the proper description of the angle-resolved photoemission spectra cannot be done by the LSDA but by LSDA+DMFT.[39] In the case of Fe, a broad contribution of the LSDA+DMFT MCP is also obtained in the energy range [−1.0 Ry, −0.4 Ry], and consequently a similar tendency of localization of the spin density is expected.

IV. CONCLUSIONS

In conclusion, the MCPs of Fe and Ni have been determined using the SPR-KKR band-structure method within the LSDA and LSDA+DMFT approach, respectively. The influence of electron correlations on the MCP of Fe and Ni [111] has been discussed. For high transfer momenta ($p_z \geqslant 2$ a.u.), no significant corrections due to dynamical electronic correlations are seen in the Compton profile, therefore the dynamics of the process can be captured equally well by a LSDA approach. In contrast, for small momentum transfer, clear evidence for the interplay between the energy transferred to the electron and the electronic correlations is seen: including the local but dynamical self-energy leads to an improved MCP spectra. In addition, the decomposition of the Ni [111] MCPs shows a large and broad contribution by the DMFT+LSDA approach stemming from the energy window between the bottom of the valence band and 0.4 Ry binding energy. For the corresponding MCP decomposition, the LSDA approach shows just a small and narrow contribution stemming from the same energy range. We consider this feature to be a consequence of the localization tendency of the spin density due to electronic correlations.

ACKNOWLEDGMENTS

D.B. acknowledge the financial support of the Deutsche Forschungsgemeinschaft through FOR 1346 and the project POSDRU 89/1.5/S/60189 with the title "Postdoctoral Programs for Sustainable Development in a Knowledge Based Society." Financial support by the Bundesministerium für Bildung und Forschung (05K10WMA) is also gratefully acknowledged.

[1] M. J. Cooper, Rep. Prog. Phys. **48**, 415 (1985).
[2] S. W. Lovesey and S. P. Collins, *X-Ray Scattering and Absorption by Magnetic Materials* (Clarendon, Oxford, 1996), Chap. 7.
[3] S. Wakoh and Y. Kubo, J. Magn. Magn. Mater. **5**, 202 (1977).
[4] Y. Kubo and S. Asano, Phys. Rev. B **42**, 4431 (1990).
[5] Y. Tanaka, N. Sakai, Y. Kubo, and H. Kawata, Phys. Rev. Lett. **70**, 1537 (1993).
[6] T. Baruah, R. R. Zope, and A. Kshirsagar, Phys. Rev. B **62**, 16435 (2000).
[7] M. A. G. Dixon, J. A. Duffy, S. Gardelis, J. E. McCarthy, M. J. Cooper, S. B. Dugdale, T. Jarlborg, and D. N. Timms, J. Phys. Condens. Matter **10**, 2759 (1998).
[8] M. Tokii and M. Matsumoto, J. Phys. Condens. Matter **18**, 3639 (2006).
[9] Z. Major, S. B. Dugdale, R. J. Watts, J. Laverock, J. J. Kelly, D. C. R. Hedley, and M. A. Alam, J. Phys. Chem. Solids **65**, 2011 (2004).
[10] Y. Kubo, J. Phys. Chem. Solids **65**, 2077 (2004).
[11] Y. Sakurai, A. Deb, M. Itou, A. Koizumi, Y. Tomioka, and Y. Tokura, J. Phys. Condens. Matter **16**, S5717 (2004).
[12] G. E. W. Bauer and J. R. Schneider, Phys. Rev. B **31**, 681 (1985).
[13] A. Liebsch, Phys. Rev. Lett. **43**, 1431 (1979).
[14] A. Liebsch, Phys. Rev. B **23**, 5203 (1981).
[15] C. S. Wang and J. Callaway, Phys. Rev. B **15**, 298 (1977).
[16] W. Eberhardt and E. W. Plummer, Phys. Rev. B **21**, 3245 (1980).
[17] D. E. Eastman, F. J. Himpsel, and J. A. Knapp, Phys. Rev. Lett. **40**, 1514 (1978).
[18] F. J. Himpsel, J. A. Knapp, and D. E. Eastman, Phys. Rev. B **19**, 2919 (1979).
[19] S. Hüfner and G. K. Wertheim, Phys. Lett. A **51**, 299 (1975).
[20] C. Guillot, Y. Ballu, J. Paigné, J. Lecante, K. P. Jain, P. Thiry, R. Pinchaux, Y. Petroff, and L. M. Falicov, Phys. Rev. Lett. **39**, 1632 (1977).
[21] E. Dietz, U. Gerhardt, and C. J. Maetz, Phys. Rev. Lett. **40**, 892 (1978).
[22] A. I. Lichtenstein, M. I. Katsnelson, and G. Kotliar, Phys. Rev. Lett. **87**, 067205 (2001).
[23] J. Minár, L. Chioncel, A. Perlov, H. Ebert, M. I. Katsnelson, and A. I. Lichtenstein, Phys. Rev. B **72**, 045125 (2005).
[24] J. Braun, J. Minár, H. Ebert, M. I. Katsnelson, and A. I. Lichtenstein, Phys. Rev. Lett. **97**, 227601 (2006).
[25] J. Minár, J. Phys. Condens. Matter **23**, 253201 (2011).
[26] L. Chioncel, L. Vitos, I. A. Abrikosov, J. Kollár, M. I. Katsnelson, and A. I. Lichtenstein, Phys. Rev. B **67**, 235106 (2003).
[27] H. Ebert, D. Ködderitzsch, and Minár, Rep. Prog. Phys. **74**, 096501 (2011).
[28] Z. Szotek, B. L. Gyorffy, G. M. Stocks, and W. M. Temmerman, J. Phys. F **14**, 2571 (1984).
[29] D. Benea, S. Mankovsky, and H. Ebert, Phys. Rev. B **73**, 094411 (2006).
[30] D. Benea, Ph.D. thesis, LMU München, 2004.
[31] S. H. Vosko, L. Wilk, and M. Nusair, Can. J. Phys. **58**, 1200 (1980).
[32] H. J. Monkhorst and J. D. Pack, Phys. Rev. B **13**, 5188 (1976).
[33] M. I. Katsnelson and A. I. Lichtenstein, Eur. Phys. J. B **30**, 9 (2002).
[34] L. V. Pourovskii, M. I. Katsnelson, and A. I. Lichtenstein, Phys. Rev. B **72**, 115106 (2005).
[35] F. Aryasetiawan, M. Imada, A. Georges, G. Kotliar, S. Biermann, and A. I. Lichtenstein, Phys. Rev. B **70**, 195104 (2004).
[36] I. Di Marco, J. Minár, S. Chadov, M. I. Katsnelson, H. Ebert, and A. I. Lichtenstein, Phys. Rev. B **79**, 115111 (2009).
[37] J. E. McCarthy, M. J. Cooper, P. K. Timms, A. Brahmia, D. Laundy, P. P. Kane, G. Clark, and D. Laundy, J. Synchr. Rad. **4**, 102 (1997).
[38] K. N. Altmann, D. Y. Petrovykh, G. J. Mankey, N. Shannon, N. Gilman, M. Hochstrasser, R. F. Willis, and F. J. Himpsel, Phys. Rev. B **61**, 15661 (2000).
[39] J. Sanchez-Barriga, J. Fink, V. Boni, I. Di Marco, J. Braun, J. Minár, A. Varykhalov, O. Rader, V. Bellini, F. Manghi, H. Ebert, M. I. Katsnelson, A. I. Lichtenstein, O. Eriksson, W. Eberhardt, and H. A. Dürr, Phys. Rev. Lett. **103**, 267203 (2009).